

Cramér–Rao Bounds for Magneto-Inductive Integrated Sensing and Communications

Haofan Dong, *Student Member, IEEE*, and Ozgur B. Akan, *Fellow, IEEE*

Abstract—Magnetic induction (MI) enables communication in RF-denied environments (underground, underwater, in-body), where the medium conductivity imprints a deterministic signature on the channel. This letter derives a closed-form Cramér–Rao bound (CRB) for the joint estimation of range and medium conductivity from MI pilot observations in an integrated sensing and communication (ISAC) framework. The Fisher information matrix reveals that the joint estimation penalty converges to 3 dB in the near-field regime, meaning conductivity sensing adds at most a factor-of-two loss in ranging precision. Monte Carlo maximum-likelihood simulations confirm that the CRB is achievable under practical operating conditions.

Index Terms—Magnetic induction, integrated sensing and communication (ISAC), Cramér–Rao bound, joint parameter estimation, underground communication.

I. INTRODUCTION

Integrated sensing and communication (ISAC) has attracted considerable attention as an enabling technology for sixth-generation (6G) wireless systems, allowing a single waveform to serve both data transmission and environmental perception [1], [2]. Current ISAC research, however, predominantly focuses on radio-frequency (RF) links operating at millimeter-wave or sub-terahertz bands, where the sensing function relies on target echoes to extract range, velocity, and angle [1], [3]. These RF-centric designs implicitly assume free-space or near-free-space propagation and therefore break down in lossy, RF-denied media such as soil, seawater, and biological tissue, where electromagnetic waves suffer prohibitive attenuation.

Magnetic induction (MI) communication offers a distinct physical layer for such environments. Unlike far-field RF propagation, MI exploits near-field inductive coupling between coils, with a quasi-static magnetic field that is largely immune to multipath fading and experiences negligible change in medium permeability [4], [5]. These properties have made MI a candidate technology for wireless underground sensor networks (WUSNs) [6], [7]. A recent framework termed magneto-inductive ISAC (MI-ISAC) has shown that the deterministic MI channel structure enables joint communication and sensing in RF-denied environments [8]. Notably, the MI channel response carries a bijective imprint of the surrounding medium conductivity σ_m through eddy-current-induced attenuation and phase rotation [4]. This physics offers a natural opportunity for opportunistic sensing [9]: just as commercial microwave links

H. Dong and O. B. Akan are with the Internet of Everything Group, Department of Engineering, University of Cambridge, Cambridge CB3 0FA, U.K. (e-mail: hd489@cam.ac.uk; oba21@cam.ac.uk).

Ozgur B. Akan is also with the Center for neXt-generation Communications (CXC), Department of Electrical and Electronics Engineering, Koç University, 34450 Istanbul, Turkey (email: oba21@cam.ac.uk)

have been repurposed to monitor rainfall from signal attenuation, an MI communication link can simultaneously sense the medium it traverses without dedicated sensing hardware. The sensed conductivity is of direct practical value: in precision agriculture, soil conductivity correlates with moisture content and salinity [6]; in pipeline monitoring, conductivity changes indicate fluid composition or corrosion onset [7].

Despite this potential, existing MI literature treats medium conductivity exclusively as a known system parameter. Channel models [4], [5] and network optimization [7] assume σ_m is given *a priori*, while MI localization studies derive Cramér–Rao bounds (CRBs) for position coordinates with σ_m held fixed [10]. While [8] established the MI-ISAC framework for geometric parameter estimation, it did not address the joint range–conductivity problem nor quantify the estimation penalty when both must be resolved simultaneously. The recent comprehensive survey by Ma *et al.* [5] explicitly identifies integrated MI communication, navigation, and sensing as an open research direction, further motivating this investigation.

In this letter, we extend the MI-ISAC framework to joint range–conductivity estimation and develop its estimation-theoretic analysis. The main contributions are:

- 1) A closed-form Fisher information matrix (FIM) is derived for joint range and conductivity estimation from MI pilots, revealing how geometric spreading and eddy-current absorption contribute separable information.
- 2) An analytical penalty formula shows the CRB increase due to joint estimation converges to 3 dB in the near-field regime, i.e., at most a factor-of-two loss in ranging precision.
- 3) Monte Carlo MLE simulations (5000 trials) validate the CRB achievability.

II. SYSTEM MODEL

A. MI-ISAC Scenario

We consider a magnetic induction (MI) link between two coaxial coil transceivers embedded in a lossy medium (Fig. 1). Each coil has radius a and N turns; the coils are separated by distance r in a medium of unknown conductivity σ_m . The transmitter sends known pilots that serve both communication and channel estimation [4], [7].

B. MI Channel Model

The mutual inductance between two coaxial circular coils in a homogeneous lossy medium with conductivity σ_m and permeability μ_0 is [4], [11]

$$M(r, \sigma_m) = \frac{\mu_0 \pi N^2 a^4}{2 r^3} e^{-(1+j) \alpha r}, \quad (1)$$

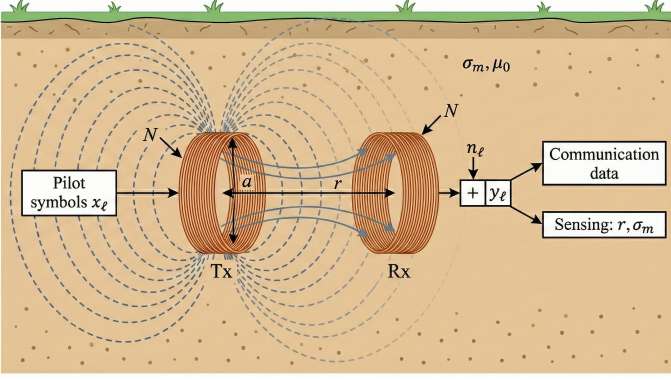


Fig. 1. MI-ISAC system model. Two coaxial coils (radius a , N turns) are separated by range r in a lossy medium (conductivity σ_m , permeability μ_0). The transmitter sends L pilot symbols; the receiver jointly estimates $\theta = [r, \sigma_m]^T$ from the received signal, while also decoding communication data.

where

$$\alpha(\sigma_m) = \sqrt{\pi f_0 \mu_0 \sigma_m} \quad (2)$$

is the field attenuation constant at operating frequency f_0 , and the skin depth is $\delta = 1/\alpha$. The exponential factor in (1) captures the eddy-current loss: the real part of the exponent models amplitude decay, while the imaginary part introduces a phase shift that grows with the electrical distance αr .

It is convenient to introduce the dimensionless parameter

$$\kappa r \triangleq \sqrt{2} \alpha r = r \sqrt{2 \pi f_0 \mu_0 \sigma_m}, \quad (3)$$

which quantifies the ratio of coil separation to skin depth. The regime $\kappa r \ll 1$ corresponds to the *near field* where medium loss is negligible, while $\kappa r \gg 1$ indicates heavy attenuation.

The normalized complex channel gain observed at the receiver is

$$h(r, \sigma_m) = \frac{\omega M(r, \sigma_m)}{Z_{\text{ref}}} = \frac{C}{r^3} e^{-(1+j)\alpha r}, \quad (4)$$

where $\omega = 2\pi f_0$, Z_{ref} is a reference impedance that normalizes the voltage transfer, and $C \triangleq \omega \mu_0 \pi N^2 a^4 / (2 Z_{\text{ref}})$ absorbs all frequency- and geometry-dependent constants. Note that h depends on the two unknowns (r, σ_m) through the near-field decay r^{-3} and the exponential medium loss $e^{-(1+j)\alpha r}$, respectively.

C. Signal Model

The transmitter sends L pilot symbols $\{x_\ell\}_{\ell=1}^L$ with per-symbol power $P_{\text{tx}} = \mathbb{E}[|x_\ell|^2]$. The received signal at the ℓ -th pilot is

$$y_\ell = h(r, \sigma_m) x_\ell + n_\ell, \quad \ell = 1, \dots, L, \quad (5)$$

where $n_\ell \sim \mathcal{CN}(0, N_0 B)$ is additive white Gaussian noise with power spectral density N_0 and bandwidth B . The channel h is treated as constant over the L pilot symbols (quasi-static assumption), which is well justified for MI links where the near-field coupling changes only with the physical displacement of the coils [4].

Since the pilot waveform is known, the matched-filter sufficient statistic for h is [12]

$$\hat{h}_{\text{MF}} = \frac{\sum_{\ell=1}^L y_\ell x_\ell^*}{\sum_{\ell=1}^L |x_\ell|^2} = h(r, \sigma_m) + \tilde{n}, \quad (6)$$

where $\tilde{n} \sim \mathcal{CN}(0, N_0 B / (L P_{\text{tx}}))$. The observation \hat{h}_{MF} contains all information about the parameter vector

$$\theta = \begin{bmatrix} r \\ \sigma_m \end{bmatrix} \in \mathbb{R}_{>0}^2 \quad (7)$$

that is available in the pilot data.

D. Problem Formulation

The goal is to characterize the fundamental estimation accuracy for the *joint* recovery of θ from (6) via the Cramér–Rao bound (CRB). Specifically, for any unbiased estimator $\hat{\theta}$, $\mathbb{E}[(\hat{\theta} - \theta)(\hat{\theta} - \theta)^T] \succeq \mathbf{J}^{-1}(\theta)$, where $\mathbf{J}(\theta)$ is the 2×2 Fisher information matrix (FIM). The *joint estimation penalty* is defined as

$$\Delta_r \triangleq \frac{\text{CRB}_r^{\text{joint}}}{\text{CRB}_r^{\text{single}}} = \frac{[\mathbf{J}^{-1}]_{11}}{1/J_{11}} \geq 1, \quad (8)$$

where $\text{CRB}_r^{\text{single}} = 1/J_{11}$ is the bound when σ_m is known. The penalty Δ_r quantifies how much harder it is to estimate range when the medium conductivity must be simultaneously inferred. The penalty for σ_m is defined analogously. Note that \hat{h}_{MF} provides two real degrees of freedom (amplitude and phase), which suffices for the two real unknowns (r, σ_m) ; identifiability follows from the injectivity of $h(r, \sigma_m)$ on $\mathbb{R}_{>0}^2$, since the near-field decay r^{-3} and the eddy-current phase $e^{-j\alpha r}$ impose linearly independent constraints.

III. CRAMÉR–RAO BOUND ANALYSIS

This section derives the Fisher information matrix for the joint estimation of $\theta = [r, \sigma_m]^T$ from the sufficient statistic \hat{h}_{MF} in (6), and characterizes the penalty incurred by estimating both parameters simultaneously.

Since $\hat{h}_{\text{MF}} \sim \mathcal{CN}(h(\theta), N_0 B / (L P_{\text{tx}}))$, the (i, j) -th entry of the 2×2 FIM for the deterministic (non-random) parameter vector θ is [12]

$$J_{ij} = \frac{2 L P_{\text{tx}}}{N_0 B} \text{Re} \left[\frac{\partial h}{\partial \theta_i} \frac{\partial h^*}{\partial \theta_j} \right]. \quad (9)$$

The required partial derivatives of h in (4) are

$$\frac{\partial h}{\partial r} = h(r, \sigma_m) [-\beta - j\alpha], \quad (10)$$

$$\frac{\partial h}{\partial \sigma_m} = h(r, \sigma_m) \left[-(1+j) \frac{\alpha r}{2\sigma_m} \right], \quad (11)$$

where $\beta \triangleq 3/r + \alpha$ and we have used $\partial \alpha / \partial \sigma_m = \alpha / (2\sigma_m)$ from (2). The derivative (10) contains a real part β arising from the near-field decay r^{-3} and the attenuation $e^{-\alpha r}$, and an imaginary part α from the medium-induced phase rotation. The derivative (11) is proportional to $(1+j)$, reflecting the equal sensitivity of the channel amplitude and phase to changes in σ_m .

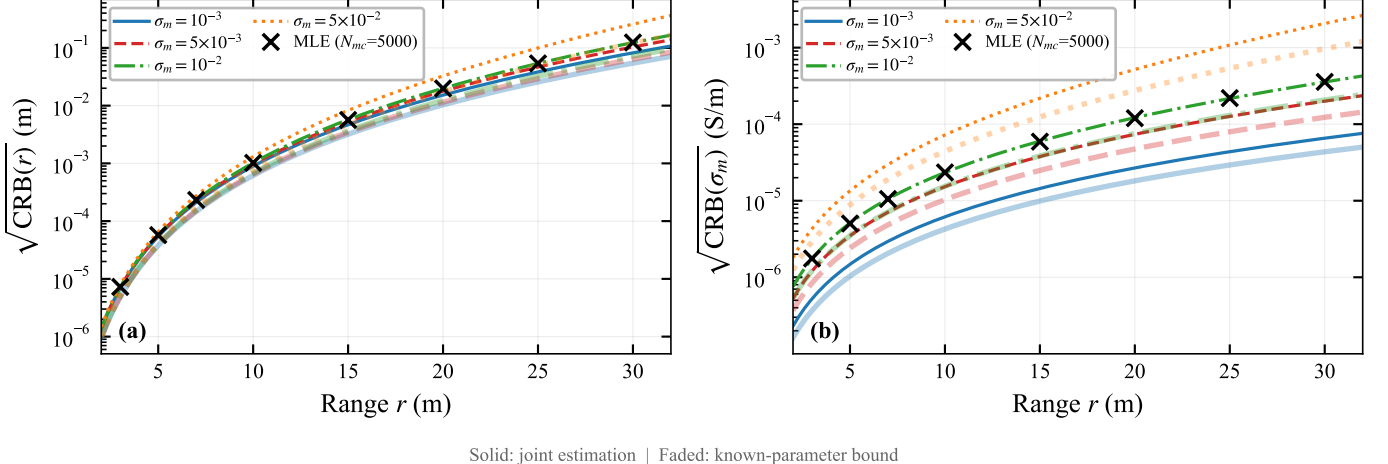


Fig. 2. Joint vs. single-parameter CRB for (a) range and (b) conductivity estimation across four medium types. Solid: joint estimation; faded: known-parameter bound. Cross markers: MLE with $N_{mc} = 5000$.

Substituting (10)–(11) into (9) and factoring $\gamma \triangleq 2LP_{tx}|h|^2/(N_0B)$, the FIM takes the form

$$\mathbf{J} = \gamma \begin{bmatrix} \beta^2 + \alpha^2 & \frac{\alpha r}{2\sigma_m} (\beta + \alpha) \\ \frac{\alpha r}{2\sigma_m} (\beta + \alpha) & \frac{\alpha^2 r^2}{2\sigma_m^2} \end{bmatrix}. \quad (12)$$

The off-diagonal term is nonzero whenever $\alpha > 0$ (i.e., $\sigma_m > 0$), indicating that range and conductivity estimation are inherently coupled through the medium loss. The following result characterizes this coupling.

Theorem 1. Let ρ denote the FIM correlation coefficient $\rho \triangleq J_{12}/\sqrt{J_{11} J_{22}}$. Then

$$\rho(\alpha r) = \frac{3 + 2\alpha r}{\sqrt{2[(3 + \alpha r)^2 + (\alpha r)^2]}}, \quad (13)$$

and the joint estimation penalties for r and σ_m are

$$\Delta_r = \Delta_{\sigma_m} = \frac{1}{1 - \rho^2} \geq 1. \quad (14)$$

Proof: The diagonal and off-diagonal entries of \mathbf{J} in (12) yield $J_{11} = \gamma(\beta^2 + \alpha^2)$, $J_{22} = \gamma\alpha^2 r^2/(2\sigma_m^2)$, and $J_{12} = \gamma\alpha r(\beta + \alpha)/(2\sigma_m)$. Direct computation gives $J_{12}^2/(J_{11} J_{22}) = (\beta + \alpha)^2/[2(\beta^2 + \alpha^2)]$, which equals ρ^2 in (13) after substituting $\beta = 3/r + \alpha$. For any 2×2 positive-definite matrix, the inverse satisfies $[\mathbf{J}^{-1}]_{ii} = J_{jj}/\det(\mathbf{J})$, so $\Delta_r = J_{11}[\mathbf{J}^{-1}]_{11} = J_{11}J_{22}/\det(\mathbf{J}) = 1/(1 - \rho^2)$. The same identity holds for Δ_{σ_m} by symmetry. ■

Corollary 1 (Near-field limit). As $\alpha r \rightarrow 0$ (equivalently $\kappa r \rightarrow 0$), the correlation coefficient satisfies $\rho \rightarrow 1/\sqrt{2}$, and hence

$$\lim_{\kappa r \rightarrow 0} \Delta_r = \lim_{\kappa r \rightarrow 0} \Delta_{\sigma_m} = 2 \quad (\text{i.e., } 3.01 \text{ dB}). \quad (15)$$

This follows by setting $\alpha r = 0$ in (13), giving $\rho = 3/\sqrt{18} = 1/\sqrt{2}$.

The 3 dB penalty has a geometric origin: as $\kappa r \rightarrow 0$, $\partial h/\partial r$ is dominated by the real-valued decay r^{-3} while $\partial h/\partial \sigma_m$ retains its $(1 + j)$ structure, fixing their angle in the complex plane at $\rho = 1/\sqrt{2}$ independent of system parameters.

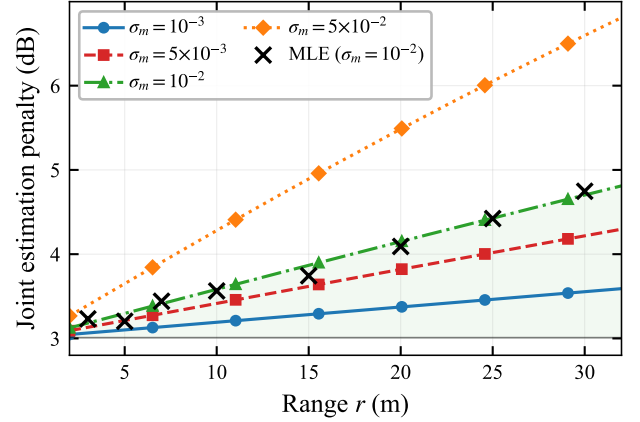


Fig. 3. Joint estimation penalty vs. range for four medium conductivities. Horizontal line: 3 dB near-field limit. Cross markers: MLE empirical penalty ($N_{mc} = 5000$, $\sigma_m = 0.01 \text{ S/m}$).

Remark: In the opposite limit $\alpha r \rightarrow \infty$, (13) gives $\rho \rightarrow 1$, and the penalty diverges. Physically, both partial derivatives become proportional to $(1 + j)h e^{-(1+j)\alpha r}$, so their “directions” in the complex plane align and the FIM becomes rank-deficient; r and σ_m are then asymptotically indistinguishable from a single observation. This motivates operating in the regime $\kappa r < 1$, where the penalty remains below approximately 5 dB (see Section IV).

IV. NUMERICAL RESULTS

The analytical CRB and penalty results are validated through Monte Carlo simulations with maximum likelihood estimation (MLE). Unless stated otherwise, the default parameters are: operating frequency $f_0 = 10 \text{ kHz}$, coil radius $a = 0.15 \text{ m}$, number of turns $N = 20$, pilot count $L = 100$, transmit power $P_{tx} = 0 \text{ dBm}$, and noise bandwidth $B = 1 \text{ kHz}$ at temperature $T_0 = 290 \text{ K}$. The MLE is implemented via multi-start Nelder–Mead optimization of the negative log-likelihood $\mathcal{L}(\boldsymbol{\theta}) = L |\hat{h}_{\text{MF}} - h(\boldsymbol{\theta})|^2/(N_0 B)$, with $N_{mc} = 5000$ independent trials per operating point.

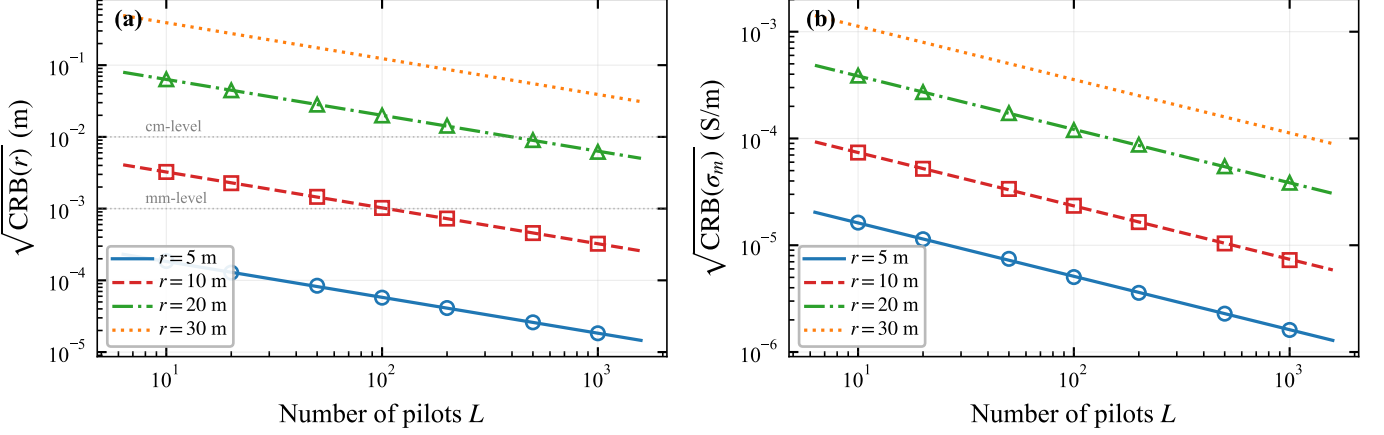


Fig. 4. CRB vs. pilot count L for (a) range and (b) conductivity estimation at multiple distances ($\sigma_m = 0.01$ S/m). Open markers: MLE validation. Dashed lines: cm- and mm-level accuracy thresholds.

Fig. 2 compares the joint CRB (solid) with the known-parameter bound (faded) for four conductivities. The MLE variance (crosses, $\sigma_m = 0.01$ S/m) tracks the joint CRB, and a consistent ≈ 3 dB gap is visible across all media, confirming Theorem 1.

Fig. 3 shows the penalty versus range. All curves converge to the 3 dB floor at short range; higher conductivity causes faster growth due to larger κr . For typical underground conditions ($\sigma_m \in [10^{-3}, 10^{-1}]$ S/m, $r < 20$ m), the penalty stays below 5 dB.

Fig. 4 illustrates the system design space by plotting $\sqrt{\text{CRB}}$ against the pilot count L for multiple ranges. Both range and conductivity estimation accuracy improve as $1/\sqrt{L}$, consistent with the L -scaling in (9). At $r = 10$ m, centimeter-level range accuracy is achievable with $L \geq 50$ pilots, while $r = 20$ m requires $L \geq 200$. The MLE markers (open symbols) match the analytical curves across the full sweep, validating the CRB achievability for all tested configurations.

V. CONCLUSION

This letter has derived closed-form Cramér–Rao bounds for joint range and medium conductivity estimation in magneto-inductive ISAC systems. The analysis reveals a fundamental 3 dB joint estimation penalty in the near-field regime, showing that range and conductivity remain distinguishable owing to the distinct information contributions of geometric spreading and eddy-current absorption. Monte Carlo MLE simulations confirm the tightness of the bound across the tested parameter space. Future work will extend the analysis to multi-coil arrays, frequency-diverse pilots, and experimental validation in field-deployed underground sensor networks.

REFERENCES

- [1] F. Liu, Y. Cui, C. Masouros, J. Xu, T. X. Han, Y. C. Eldar, and S. Buzzi, “Integrated sensing and communications: Toward dual-functional wireless networks for 6G and beyond,” *IEEE J. Sel. Areas Commun.*, vol. 40, no. 6, pp. 1728–1767, Jun. 2022.
- [2] J. A. Zhang, M. L. Rahman, K. Wu, X. Huang, Y. J. Guo, S. Chen, and J. Yuan, “An overview of signal processing techniques for joint communication and radar sensing,” *IEEE J. Sel. Topics Signal Process.*, vol. 15, no. 6, pp. 1295–1315, Nov. 2021.
- [3] A. Liu, Z. Huang, M. Li, Y. Wan, W. Li, T. X. Han, C. Liu, R. Du, D. K. P. Tan, J. Lu, Y. Shen, F. Colone, and K. Chetty, “A survey on fundamental limits of integrated sensing and communication,” *IEEE Commun. Surveys Tuts.*, vol. 24, no. 2, pp. 994–1034, 2022.
- [4] Z. Sun and I. F. Akyildiz, “Magnetic induction communications for wireless underground sensor networks,” *IEEE Trans. Antennas Propag.*, vol. 58, no. 7, pp. 2426–2435, Jul. 2010.
- [5] H. Ma, E. Liu, W. Ni, Z. Fang, R. Wang, Y. Gao, D. Niyato, and E. Hossain, “Through-the-Earth magnetic induction communication and networking: A comprehensive survey,” *IEEE Commun. Surveys Tuts.*, vol. 28, pp. 2263–2305, 2025.
- [6] N. Saeed, M.-S. Alouini, and T. Y. Al-Naffouri, “Toward the Internet of underground things: A systematic survey,” *IEEE Commun. Surveys Tuts.*, vol. 21, no. 4, pp. 3443–3466, 2019.
- [7] S. Kisseleff, I. F. Akyildiz, and W. H. Gerstacker, “Survey on advances in magnetic induction-based wireless underground sensor networks,” *IEEE Internet Things J.*, vol. 5, no. 6, pp. 4843–4856, Dec. 2018.
- [8] H. Dong and O. B. Akan, “MI-ISAC: Magneto-inductive integrated sensing and communication in the reactive near-field for RF-denied environments,” *arXiv preprint arXiv:2602.07714*, Feb. 2026, submitted to IEEE Wireless Commun. Lett.
- [9] H. Messer, A. Zinevich, and P. Alpert, “Environmental monitoring by wireless communication networks,” *Science*, vol. 312, no. 5774, p. 713, May 2006.
- [10] N. Saeed, M.-S. Alouini, and T. Y. Al-Naffouri, “3D localization for Internet of underground things in oil and gas reservoirs,” *IEEE Access*, vol. 7, pp. 121 769–121 780, 2019.
- [11] I. F. Akyildiz, P. Wang, and Z. Sun, “Realizing underwater communication through magnetic induction,” *IEEE Commun. Mag.*, vol. 53, no. 11, pp. 42–48, Nov. 2015.
- [12] S. M. Kay, *Fundamentals of Statistical Signal Processing: Estimation Theory*. Upper Saddle River, NJ, USA: Prentice-Hall, 1993.